Interfacial and bulk spin Hall contributions to fieldlike spin-orbit torque generated by iridium

Sutapa Dutta [1,2] Arnab Bose [1,*] A. A. Tulapurkar,[2] R. A. Buhrman,[1] and D. C. Ralph[3,4]

[1]*School of Applied and Engineering Physics, Cornell University, New York 14853, USA*
[2]*Department of Electrical Engineering, Indian Institute of Technology Bombay, Mumbai 400076, India*
[3]*Laboratory of Atomic and Solid State Physics, Cornell University, New York 14853, USA*
[4]*Kavli Institute at Cornell for Nanoscale Science, Ithaca, New York 14853, USA*

We present measurements of spin-orbit torques generated by Ir as a function of film thickness in sputtered Ir/CoFeB and Ir/Co samples. We find that Ir provides a dampinglike component of spin-orbit torque with a maximum spin-torque conductivity $\sigma_{\mathrm{DL}}^{\mathrm{eff}} = (1.4 \pm 0.1) \times 10^5 \frac{\hbar}{2e} \Omega^{-1}\,\mathrm{m}^{-1}$ and a maximum spin-torque efficiency of $\xi_{DL} = 0.042 \pm 0.005$, which is sufficient to drive switching in a 0.8 nm film of CoFeB with perpendicular magnetic anisotropy. We also observe a surprisingly large fieldlike spin-orbit torque (FLT). Measurements as a function of Ir thickness indicate a substantial contribution to the FLT from an interface mechanism, so that in the ultrathin limit there is a nonzero FLT with a maximum torque conductivity $\sigma_{\mathrm{FL}}^{\mathrm{eff}} = -(5.0 \pm 0.5) \times 10^4 \frac{\hbar}{2e} \Omega^{-1}\,\mathrm{m}^{-1}$. When the Ir film thickness becomes comparable to or greater than its spin diffusion length, 1.6 ± 0.3 nm, there is also a smaller bulk contribution to the fieldlike torque.

I. INTRODUCTION

Spin-orbit interactions (SOIs) play a central role in the development of next-generation spintronic devices for nonvolatile magnetic random-access memory (MRAM) applications [1,2]. Heavy metals with large SOI such as Pt [3,4], Ta [5–7], and W [8–10] are efficient generators of spin current to produce spin-orbit torques (SOTs) on an adjacent magnetic layer. Iridium (Ir) is another heavy metal with a large SOI [11], which has been used to realize skyrmions and chiral domain wall structures as it can provide a strong interfacial Dzyaloshinskii-Moriya interaction (DMI) [12]. Recently it has been reported that Ir is also capable of converting charge current into spin current, with a dampinglike torque efficiency $\xi_{DL} = 0.005$–0.01 (where $\xi_{DL} \equiv \tau_{\mathrm{DL}}/J_C = T_{\mathrm{int}}\theta_{\mathrm{SH}}$, with τ_{DL} the spin-orbit torque per unit area, J_C the applied current density, T_{int} an interface spin transparency factor, and θ_{SH} the spin Hall ratio within the heavy metal), as measured by current-induced domain wall motion [13], hysteresis loop shifts [14], and second-harmonic Hall measurements [15]; $\theta_{\mathrm{SH}} \approx 0.02$ as measured by spin pumping [16,17]. Magnetic switching driven by spin-orbit torque from Ir has also been observed [15,18]. Here, we use spin-torque ferromagnetic resonance (ST FMR) and second-harmonic Hall (SHH) measurements to confirm that Ir exhibits a sizable charge to spin current conversion efficiency, with a maximum dampinglike spin-torque conductivity, $\sigma_{\mathrm{DL}}^{\mathrm{eff}} = (1.4 \pm 0.1) \times 10^5 \frac{\hbar}{2e} \Omega^{-1}\,\mathrm{m}^{-1}$ (where $\sigma_{\mathrm{DL}}^{\mathrm{eff}} \equiv \frac{\hbar}{2e}\xi_{DL}/\rho_{\mathrm{Ir}}$, with ρ_{Ir} the resistivity of the Ir) and a maximum ξ_{DL} of 0.042 ± 0.005, slightly higher than previous reports. We also observe a substantial fieldlike torque (FLT). By varying the thickness of Ir from 1.2 to 5 nm we find a dominant interface contribution to the FLT, in addition to a smaller conventional bulk contribution that grows with film thickness on the scale of the spin diffusion length.

Spin-current generation and spin-orbit torques in heavy metal (HM)/ferromagnet (FM) structures can in principle arise from either a bulk spin Hall effect (SHE) in the HM or interfacial SOI present at the interface [1,2]. Either type of effect can produce both a dampinglike torque (DLT) ($\boldsymbol{\tau}_{\mathrm{DL}} \propto \boldsymbol{m} \times \boldsymbol{\sigma_y} \times \boldsymbol{m}$) and a fieldlike torque (FLT) ($\boldsymbol{\tau}_{\mathrm{FL}} \propto \boldsymbol{m} \times \boldsymbol{\sigma_y}$) (where $\boldsymbol{\sigma_y}$ is the orientation of a current-induced spin, in plane and perpendicular to the current). First-principles calculations generally suggest that the bulk SHE should produce a DLT greater than the FLT since the real part of the interfacial spin mixing conductance (G_r) is larger than the imaginary part (G_i) [19,20]. Experimentally, it is possible to separate out the interface-driven and the bulk SHE driven SOTs by varying the thickness of the HM [21,22]. We model the thickness dependence of the spin-orbit torque conductivity as approximately (this form assumes that spin back flow is not strongly thickness dependent) [23,24]

$$\sigma_{\mathrm{SOT}} = \sigma_{\mathrm{SOT}}^{\mathrm{interface}} + \sigma_{\mathrm{SOT}}^{\mathrm{bulk}}\left(1 - \mathrm{sech}\frac{t_{\mathrm{HM}}}{\lambda_{\mathrm{HM}}}\right). \qquad (1)$$

We have measured four different sets of samples. Set 1: Ti(1)/Ir(3)/Co(2–6)/Ta(1.2), set 2: Ti(1)/Ir(1–5)/CoFeB (2.3)/Ta(1.2), set 3: Ti(1)/Ir(1–5)/Co(2.3)/Ta(1.2), and set 4: Ti(1)/Ir(1–5)/CoFeB(2.3)/Ir(1.2)/Ta(1.2). (The numbers in parentheses are thicknesses in nanometers and the stoichiometry of the CoFeB layers is Co$_{20}$Fe$_{60}$B$_{20}$.) The heterostructures are deposited by magnetron sputtering using an Ar pressure of 2 mTorr, in a system with a base pressure less than 2×10^{-8} Torr. The 1 nm Ti layer acts as a seed layer to give smooth films, and the 1.2 nm Ta layer provides capping to
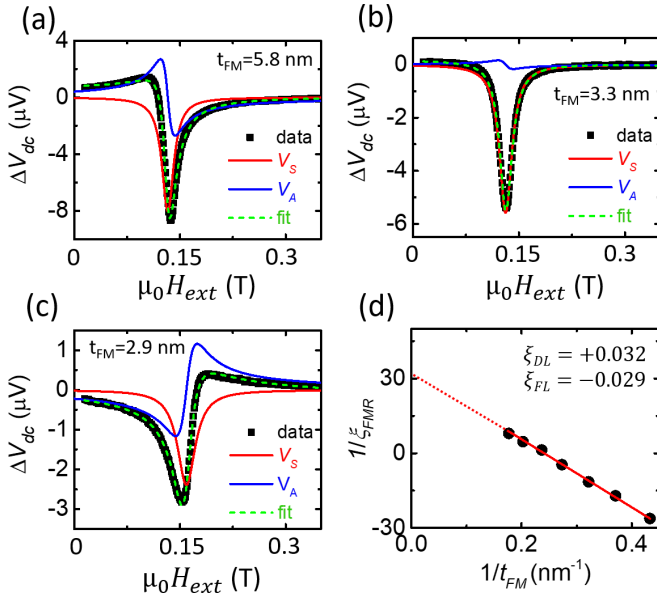
*ab2729@cornell.edu

FIG. 1. (a)–(c) ST FMR voltage signals for Ir(3 nm)/Co(t_{FM}) samples measured at a microwave frequency $f = 12$ GHz, for samples with $t_{FM} = 5.8$, 3.3, and 2.9 nm. A constant background offset voltage is subtracted in each panel. Red lines show fits to the symmetric Lorentzian component, blue lines are fits to the antisymmetric component, and green dotted lines the total fit. (d) Fit to Eq. (2) used to determine the spin-torque efficiencies.

prevent oxidation of the magnetic layer. Optical lithography and argon ion milling are used to pattern $30 \times 20 \ \mu m^2$ wires with microwave-compatible electrodes for ST FMR measurements and Hall bars ($20 \times 6 \ \mu m^2$) for the SHH and switching experiments. Devices of set 1 are used for the ST FMR measurement [25] to quantify the spin-torque ratios for the DLT (ξ_{DL}) and FLT (ξ_{FL}) for 3 nm thick Ir. We use sets 2 and 3 to perform SHH measurements [26–28] of the SOTs over a wide range of Ir thickness for a fixed thickness of FM. Set 4 provides experimental controls, to verify the distinct contributions of interfacial and bulk SOTs. All measurements are performed at room temperature.

II. ST FMR MEASUREMENTS FOR 3 nm IR FILMS

For the ST FMR measurements [23,25], a radio frequency (rf) current is applied which drives the magnet into resonance. Due to mixing of the oscillating current and the time-varying anisotropic magnetoresistance, a dc voltage is generated which is measured by a lock-in amplifier as a function of external in-plane magnetic-field sweep at an angle ϕ relative to the current direction (typically $\phi = 45°$). ST FMR signals obtained for different thicknesses of Co in Ir(3)/Co samples are shown Figs. 1(a)–1(c). These can be well fit by the sum of a symmetric Lorentzian (V_S) [red curve in Figs. 1(a)–1(c)] and antisymmetric Lorentzian (V_A) [blue curve in Figs. 1(a)–1(c)] plus a field-independent background, with $V_S = S[\frac{\Delta^2}{(H-H_0)^2+\Delta^2}]$, $V_A = A[\frac{(H-H_0)\Delta}{(H-H_0)^2+\Delta^2}]$. The amplitudes S and A are related to the in-plane and out of plane current induced torques, Δ is the linewidth, and H_0 is the resonant field.

We extract the dampinglike and fieldlike spin-torque efficiencies from the ST FMR measurements using the method of Ref. [25]. For each sample with a different Co thickness, we first define an intermediate parameter $\xi_{FMR} \equiv \frac{S}{A}(\frac{e}{\hbar})\mu_0 M_s t_{FM} t_{Ir} \sqrt{1 + (H_\perp/H_0)}$, where μ_0 is the permeability, M_S is the saturation magnetization as measured by vibrating sample magnetometry, t_{FM} is the Co thickness, t_{Ir} is the Ir thickness, and $H_\perp$ is the out of plane demagnetization field determined from the resonant field. (Values of M_S and $H_\perp$ are plotted in the Supplemental Material [29].) Assuming that the spin-torque efficiencies do not depend on the thickness of the Co layer in the range we study, the dampinglike and fieldlike spin-torque efficiencies can then be determined via a linear fit of $1/\xi_{FMR}$ to $1/t_{FM}$ [25] [Fig. 1(d)]:

$$\frac{1}{\xi_{FMR}} = \frac{1}{\xi_{DLT}}\left(1 + \frac{\hbar}{e}\frac{\xi_{FLT}}{\mu_0 M_s t_{FM} t_{Ir}}\right). \tag{2}$$

Based on this analysis, we find $\xi_{DL} = 0.032 \pm 0.004$ and $\xi_{FL} = -0.029 \pm 0.003$ for the Ir(3 nm)/Co samples. The positive sign of the DLT denotes the same sign as in Pt, while the negative sign of the FLT indicates that it is opposite to the average torque produced by the in-plane Oersted field. We find it surprising that Ir generates such a large FLT, comparable to W [30,31] even though the DLT in Ir is much smaller than in Pt [24,25] and W [8,30]. The large size of the FLT is evident already from the raw data in Fig. 1, in that the sign of the antisymmetric ST FMR component is opposite in the 2.9 nm Co sample compared to the 3.3 nm and 5.8 nm samples, indicating that in the 2.9 nm sample the spin-orbit FLT is stronger than the average torque due to the Oersted field (the torque from the Oersted field is proportional to the FM thickness while the spin-orbit torque is independent of FM thickness). The same results can be expressed in terms of effective spin-torque conductivities of the DLT $\sigma_{DL}^{eff} = \frac{\hbar}{2e}\xi_{DL}/\rho_{Ir}$ and FLT $\sigma_{FL}^{eff} = \frac{\hbar}{2e}\xi_{FL}/\rho_{Ir}$, where $\rho_{Ir} = 49 \times 10^{-8} \ \Omega$ m is the resistivity of the 3 nm Ir film in this bilayer. We find $\sigma_{DL}^{eff} = (6.5 \pm 0.8) \times 10^4 \frac{\hbar}{2e}\Omega^{-1} m^{-1}$ and $\sigma_{FL}^{eff} = (-5.9 \pm 0.8) \times 10^4 \frac{\hbar}{2e}\Omega^{-1} m^{-1}$ for the 3 nm Ir samples.

III. SECOND-HARMONIC HALL MEASUREMENTS TO DETERMINE THE DEPENDENCE OF THE TORQUE EFFICIENCIES ON Ir THICKNESS

In the SHH measurements [26–28], a low-frequency (1327 Hz in our experiment) ac current is applied and the Hall voltages (both first and second harmonic) are measured using a lock-in amplifier as a function of rotating the applied magnetic field H_{ext} in the sample plane [Fig. 2(a)]. Effective magnetic fields H_{Oe}^Y, H_{FL}^Y, and H_{DL}^Z corresponding to the current-induced torques can be determined based on the amount of current-induced tilting of the magnetization as measured by the second-harmonic Hall voltage ($V_{2\omega}$) [26–28], where H_{Oe}^Y is the Oersted field and H_{FL}^Y, H_{DL}^Z are effective fields corresponding to the FLT and DLT, respectively. $V_{2\omega}$ has the form [26–28]

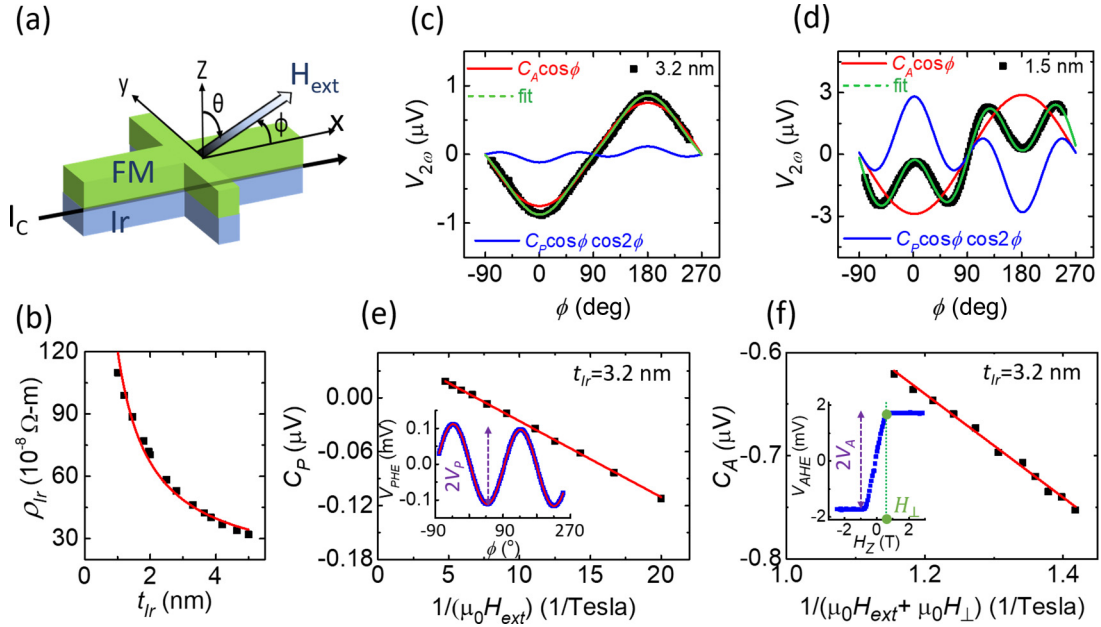$$V_{xy}^{2\omega} = C_P \cos 2\phi \cos \phi + C_A \cos \phi, \tag{3}$$

FIG. 2. (a) Sample geometry for the second-harmonic Hall measurements. (b) Ir resistivity (ρ_{Ir}) as a function of t_{Ir}. (c,d) Second-harmonic Hall voltage $V_{2\omega}$ as a function of the in-plane field angle for $\mu_0 H_{\text{ext}} = 0.05$ T, for (c) $t_{\text{Ir}} = 3.2$ nm, and (d) $t_{\text{Ir}} = 1.5$ nm. (e) Variation of C_P as a function of $1/(\mu_0 H_{\text{ext}})$. Inset of (e): Calibration of the planar Hall effect voltage (V_{PHE}) with a fit to $\sin 2\phi$. (f) Variation of C_A as a function of $1/(\mu_0 H_{\text{ext}} + \mu_0 H_\perp)$. Inset of (f): the anomalous Hall voltage (V_{AHE}) as a function of Z-field sweep.

with

$$C_P = -\left(H_{\text{FL}}^Y + H_{\text{Oe}}^Y\right)\frac{V_P}{H_{\text{ext}}} \quad \text{and}$$

$$C_A = -H_{\text{DL}}^Z \frac{V_A}{2(H_{\text{ext}} + H_\perp)} + V_{\text{ANE}} + V_{\text{ONE}}H_{\text{ext}}$$

Here V_{ANE} and V_{ONE} are constants describing the strength of the anomalous Nernst effect (ANE) and the ordinary Nernst effect (ONE), both of which can arise due to an out of plane thermal gradient. V_P is the coefficient of the planar Hall effect voltage, $V_{\text{PHE}} = V_P \sin 2\phi$, where ϕ is the in-plane angle between the magnetization (M) and the current flow direction, and V_A is the coefficient of the anomalous Hall voltage, $V_{\text{AHE}} = V_A \cos \theta$, where θ is the angle between M and the out of plane axis. We determine the value of V_P from the first-harmonic Hall signal by rotating H_{ext} in the plane [inset of Fig. 2(e)] and we obtain V_A and $H_\perp$ by sweeping H_{ext} out of plane [inset of Fig. 2(f)]. We compute the Oersted field from Ampere's law, $H_{\text{Oe}}^Y = \frac{1}{2}J_{\text{Ir}}t_{\text{Ir}}$ where J_{Ir} is the current density within the Ir layer and t_{Ir} is the Ir thickness. The current density J_{Ir} is calculated in a parallel-resistor model taking into account the thickness-dependent resistivity ρ_{Ir} of the Ir layers [Fig. 2(b)] as determined by four-probe measurements of the resistance of Ir(t_{Ir})/CoFeB(2.3) from which the resistance of the CoFeB layer ($\rho_{\text{CoFeB}} \sim 140 \times 10^{-8}$ Ω m) is subtracted. We find good consistency between these measurements of ρ_{Ir} from the Ti(1nm)/Ir(t_{Ir})/CoFeB(2.3) samples and direct measurements of Ti(1nm)/Ir(t_{Ir}) bilayers.

Figures 2(c) and 2(d) show representative second-harmonic data for samples with Ir thicknesses of 3.2 and 1.5 nm, for $\mu_0 H_{\text{ext}} = 0.05$ T. The red and blue lines represent fits to $C_A \cos \phi$ and $C_P \cos 2\phi \cos \phi$ as a function of the field

angle ϕ. $H_{\text{FL}}^Y + H_{\text{Oe}}^Y$ is determined from a fit to the magnetic-field dependence of C_P [Fig. 2(e)] and then the calculated Oersted field is subtracted, while H_{DL}^Z is determined from a fit to the magnetic-field dependence of C_A [Fig. 2(f)]. We can express the final results in terms of the effective spin-torque conductivities $\sigma_{\text{DL}}^{\text{eff}}$ and $\sigma_{\text{FL}}^{\text{eff}}$ [24,25],

$$\sigma_{\text{DL}}^{\text{eff}} = \frac{2e}{\hbar}\mu_0 M_S t_{FM}\frac{H_{\text{DL}}^Z}{E}, \tag{4}$$

$$\sigma_{\text{FL}}^{\text{eff}} = \frac{2e}{\hbar}\mu_0 M_S t_{FM}\frac{H_{\text{FL}}^Y}{E}, \tag{5}$$

where E is the longitudinal applied electric field.

It is evident already from Figs. 2(c) and 2(d) that when Ir thickness is reduced from 3.2 to 1.5 nm the strength of $H_{\text{FL}}^Y + H_{\text{Oe}}^Y$ grows dramatically relative to H_{DL}^Z, as the magnitude of the $\cos \Phi \cos 2\Phi$ component grows relative to the $\cos \Phi$ component. $H_{\text{FL}}^Y + H_{\text{Oe}}^Y$ also changes the sign when the Ir thickness is around 2.8 nm for Ir/CoFeB and 3 nm for Ir/Co (see the Supplemental Material [29]). Like the sign change as a function of FM thickness in the ST FMR measurements [Figs. 1(a)–1(c)], this can be understood as arising from a competition between the Oersted torque that scales with the Ir layer thickness and a substantial fieldlike SOT with a much weaker dependence.

The results of the SHH measurements are shown as a function of Ir thicknesses in Fig. 3 for the Ir/CoFeB(2.3 nm) sample series (left column), for the Ir/Co(2.3 nm) sample series (middle column), and for the Ir/CoFeB(2.3 nm)/Ir(1.2 nm) control samples (right column). The behavior of the damping-like spin-torque conductivities [Figs. 3(a)–3(c)] is as expected for a bulk spin Hall effect—the spin-torque conductivity goes to zero as the Ir thickness goes to zero following a
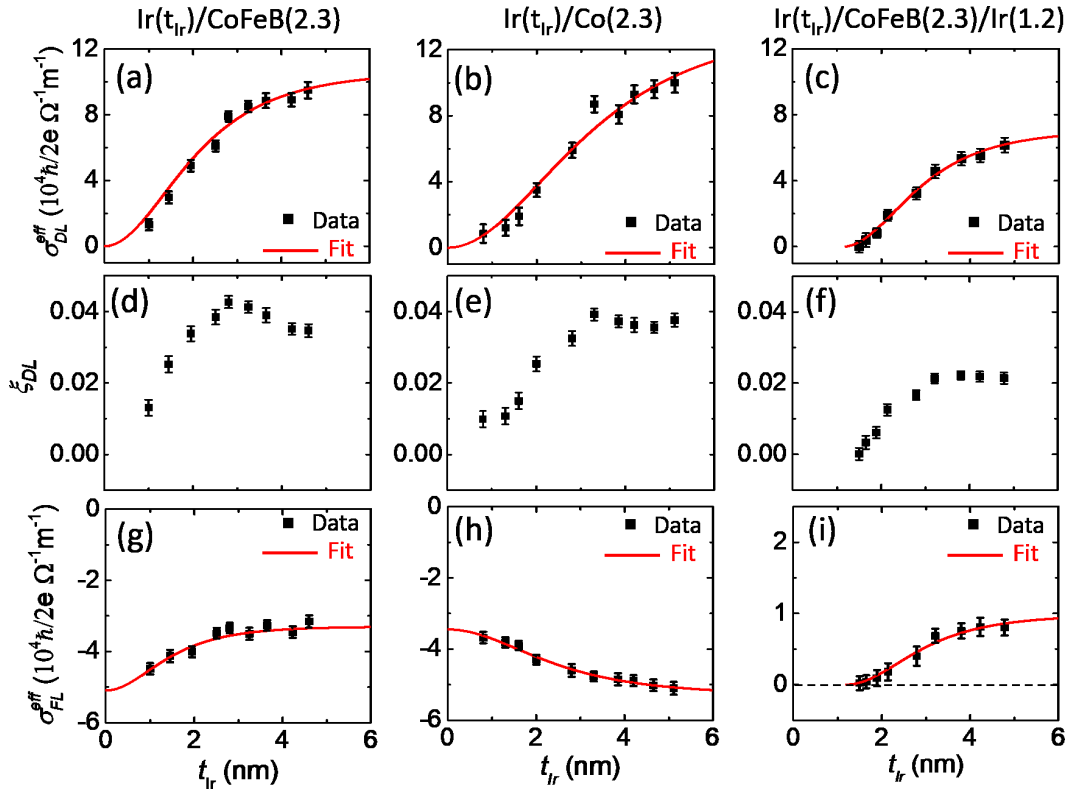
FIG. 3. Results of the second-harmonic Hall measurements of the spin-orbit torques due to Ir. (a)–(c) Dependence of the effective dampinglike spin-torque conductivity on Ir thickness for (a) the Ir/CoFeB(2.3 nm) series of samples, (b), the Ir/Co(2.3 nm) series, and (c) the Ir/CoFeB(2.3 nm)/Ir(1.2 nm) series. (d)–(f) Corresponding dampinglike spin-torque ratio as a function of Ir thickness for the three sample series. (g)–(i) Dependence of the effective fieldlike spin-torque conductivity of Ir thickness for three sample series.

reasonable fit to Eq. (1) with zero interface contribution. The values of $\sigma_{\mathrm{DL}}^{\mathrm{eff}}$ for both the Ir(3 nm)/CoFeB(2.3 nm) and the Ir(3 nm)/Co(2.3 nm) are in good quantitative agreement with the ST FMR results for the 3 nm Ir samples. At large Ir thickness, $\sigma_{\mathrm{DL}}^{\mathrm{eff}}$ saturates to the values $(1.1 \pm 0.1) \times 10^5$ $\frac{\hbar}{2e}\Omega^{-1}\,\mathrm{m}^{-1}$ for Ir/CoFeB and $(1.4 \pm 0.1) \times 10^5\,\frac{\hbar}{2e}\Omega^{-1}\,\mathrm{m}^{-1}$ for Ir/Co samples. This difference may be due to a difference in spin transparency factor for the two interfaces. Since the Ir resistivity (ρ_{Ir}) is a strong function of the Ir thickness and the spin diffusion length λ_{HM} is expected to depend on ρ_{Ir} [24], Eq. (1) is likely not strictly accurate for a single fixed value of λ_{Ir}. With this caveat, however, simple fits to Eq. (1) yield approximate spin diffusion lengths of 1.3 ± 0.2 nm for the Ir/CoFeB(2.3 nm) sample series and 1.9 ± 0.3 nm for Ir/Co(2.3 nm). Previous spin-pumping and SMR experiments found values $\lambda_{\mathrm{Ir}} \sim 0.5\text{–}1.2$ nm [14,16,17], which might depend on the resistivity and thickness [24] of the Ir films. For the Ir($t_{\mathrm{Ir}} > 1.2$ nm)/CoFeB(2.3 nm)/Ir(1.2 nm) control samples, $\sigma_{\mathrm{DL}}^{\mathrm{eff}}$ is reduced relative to the samples with a single Ir layer and goes to zero when both Ir layers have the same thickness of 1.2 nm. We ascribe this to cancellation of the contributions to the SOTs from the top and bottom Ir layers. Hence the fit starts from $t_{\mathrm{Ir}} = 1.2$ nm.

Figures 3(g) and 3(h) show the SHH results for the fieldlike spin-torque conductivity ($\sigma_{\mathrm{FL}}^{\mathrm{eff}}$) as a function of Ir thickness, along with fits to Eq. (1) using the same values of λ_{Ir} determined from the fits to $\sigma_{\mathrm{DL}}^{\mathrm{eff}}$. In striking contrast

to the dampinglike torque conductivity, $\sigma_{\mathrm{FL}}^{\mathrm{eff}}$ exhibits a dominant interface contribution, with values $\sigma_{\mathrm{FL}}^{\mathrm{interface}} = -(5.0 \pm 0.5) \times 10^4 \frac{\hbar}{2e}\Omega^{-1}\,\mathrm{m}^{-1}$ for Ir/CoFeB(2.3 nm) and $-(3.5 \pm 0.4) \times 10^4 \frac{\hbar}{2e}\Omega^{-1}\,\mathrm{m}^{-1}$ for Ir/Co(2.3 nm), along with smaller bulk values $\sigma_{\mathrm{FL}}^{\mathrm{bulk}} = 1.8 \pm 0.3) \times 10^4 \frac{\hbar}{2e}$ $\Omega^{-1}\,\mathrm{m}^{-1}$ and $-(1.6 \pm 0.2) \times 10^4 \frac{\hbar}{2e}\Omega^{-1}\,\mathrm{m}^{-1}$, respectively. The sign of $\sigma_{\mathrm{FL}}^{\mathrm{bulk}}$ is opposite for the Ir/CoFeB and Ir/Co samples, similar to the opposite signs of bulk FLT found previously for Pt/Py [32] and Pt/Co [25]. However, the interface FLT has the same sign (negative) in both Ir/CoFeB and Ir/Co. In the Ir($t_{\mathrm{Ir}} > 1.2$)/CoFeB/Ir($t_{\mathrm{Ir}} = 1.2$) control samples we observe negligible $\sigma_{\mathrm{FL}}^{\mathrm{interface}}$ and a small but nonzero $\sigma_{\mathrm{FLT}}^{\mathrm{bulk}}$ [$\sim (0.9 \pm 0.1) \times 10^3 \frac{\hbar}{2e}\Omega^{-1}\,\mathrm{m}^{-1}$] [Fig. 3(i)]. This is consistent with full cancellation of interface spin-orbit torque between the top and bottom Ir/CoFeB interfaces, and partial cancellation of the bulk spin currents for Ir layers with different thicknesses.

One must be careful in evaluating evidence of interfacial fieldlike SOTs to check that the results cannot be explained by spatial inhomogeneities in the resistivity as a function of thickness. Such inhomogeneities might give rise to a nonuniform current flow within the FM layer that produces an additional nonzero net Oersted torque. One should also be suspicious of other potential errors in subtracting off the Oersted field due to current flow in the nonmagnetic layer. We can rule out these possibilities for our samples because
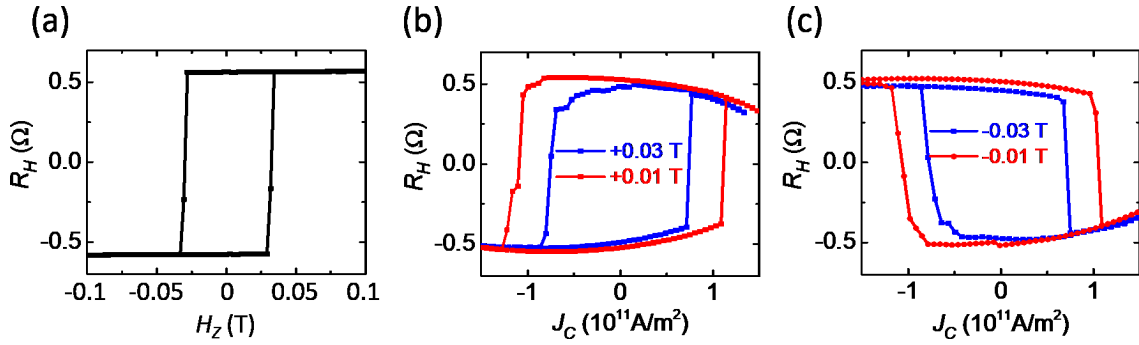
FIG. 4. (a) Anomalous Hall resistance of Ir(3)/CoFeB(0.8) as a function of an applied out of plane magnetic field. (b), (c) SOT switching as a function of applied dc current density for two different orientations of a symmetry-breaking external magnetic field ($\mu_0 H_X = \pm 0.03$ T and ± 0.01 T).

of the large magnitude of the interfacial fieldlike torque we observe. For our Ir(1)/CoFeB(2.3) samples, even if all of the current flowing through the device were localized at the interface above the CoFeB layer, this would produce a maximum in-plane Oersted field of only -0.087 mT/V, which is less than half the magnitude of the effective field that we measure corresponding to the FLT. (See details of this calculation and plots of the measured FLTs before Oersted-field subtraction in the Supplemental Material [29]). We have also verified that the current-induced SOTs are negligible in symmetrically sandwiched structures containing only a single CoFeB layer Ti(1.5)/MgO(1.5)/CoFeB(2) /MgO(1.5)/Ti(1.5).

Previous measurements of interfacial FLTs larger than the maximum possible Oersted torque have been reported in Ti/NiFe/Al$_2$O$_3$ samples [22]. Substantial interfacial FLTs have also been reported in SiN/CoFeB/Ta/TaO$_x$ samples [21], but measurements on Ta/CoFeB/MgO and TaN/CoFeB/MgO samples show much smaller values [7,33]. Kim *et al.* [34] have suggested that DMI and interface-generated spin-orbit torques can share a common origin, which is intriguing given the strong DMI from Ir. However, for Pt [24] (which is similar to Ir in providing a strong DMI), any interfacial FLT is at least a factor of 10 weaker than we find for Ir.

IV. SWITCHING APPLICATION

Finally we demonstrate current-induced SOT switching in a Ir(3)/Ti(0.4)/CoFeB(0.8)/Ti(0.2) /MgO(1.8)/Ti(1.5) heterostructure. The insertion of the 0.4 nm Ti dusting layer [35] between the Ir and the CoFeB enables perpendicular magnetic anisotropy (PMA) with a coercivity greater than 250 Oe [Fig. 4(a)] and an anisotropy field around 2.5 kOe. We observe switching of the PMA CoFeB in $20 \times 6~\mu m^2$ structures as the dc bias current is ramped [Figs. 4(b) and 4(c)] in the presence of a fixed symmetry-breaking in-plane magnetic field applied along the current direction ($\mu_0 H_x = 0.01$–0.03T). The sign of the current-induced hysteresis loop is reversed upon reversing the direction of H_x, confirming that the mechanism is SOT

switching. The minimum switching current density is just below 10^{11} A/m^2 (which corresponds to approximately 2 mA of applied dc current) at $\mu_0 H_x = 0.03$ T, comparable to previous studies in other heavy metals [1–4,36].

V. SUMMARY

We have measured both dampinglike and fieldlike spin-orbit torque generated by sputtered Ir thin films. The dampinglike torque is consistent with a conventional bulk spin Hall effect mechanism, with a maximum spin-torque conductivity $\sigma_{DL}^{eff} = (1.4 \pm 0.1) \times 10^5~\frac{\hbar}{2e}\Omega^{-1}\,m^{-1}$, a maximum spin-torque ratio $\xi_{DL} = 0.042 \pm 0.005$, and an effective spin diffusion length approximately $\lambda_{Ir} = 1.6 \pm 0.3$ nm. Unlike most other heavy metals and heavy-metal alloys we have studied, the fieldlike torque has a dominant interface origin, with $\sigma_{FL}^{interface} = -(5.0 \pm 0.5) \times 10^4~\frac{\hbar}{2e}\Omega^{-1}\,m^{-1}$ for Ir/CoFeB(2.3 nm) and $-(3.5 \pm 0.4) \times 10^4~\frac{\hbar}{2e}\Omega^{-1}\,m^{-1}$ for Ir/Co(2.3 nm), each more than a factor of 2 stronger than the bulk contributions to the FLT. Although the SOTs generated by Ir are not as suitable for applications compared to Pt, Ta, and W, they are still sufficiently strong that they should be taken into account when incorporating Ir into SOT devices to achieve a strong Dzyaloshinskii-Moriya interaction.

[1] A. Manchon, J. Železný, I. M. Miron, T. Jungwirth, J. Sinova, A. Thiaville, K. Garello, and P. Gambardella, Current-induced spin-orbit torques in ferromagnetic and antiferromagnetic systems, Rev. Mod. Phys. **91**, 035004 (2019).

[2] F. Hellman, A. Hoffmann, Y. Tserkovnyak, G. S. D. Beach, E. E. Fullerton, C. Leighton, A. H. MacDonald, D. C. Ralph, D. A. Arena, H. A. Dürr *et al.*, Interface-induced phenomena in magnetism, Rev. Mod. Phys. **89**, 025006 (2017).

[3] I. M. Miron, K. Garello, G. Gaudin, P. J. Zermatten, M. V. Costache, S. Auffret, S. Bandiera, B. Rodmacq, A. Schuhl, and P. Gambardella, Perpendicular switching of a single ferromagnetic layer induced by in-plane current injection, Nature **476**, 189 (2011).

[4] L. Liu, O. J. Lee, T. J. Gudmundsen, D. C. Ralph, and R. A. Buhrman, Current-Induced Switching of Perpendicularly Magnetized Magnetic Layers Using Spin Torque from the Spin Hall Effect, Phys. Rev. Lett. **109**, 096602 (2012).

[5] L. Liu, C.-F. Pai, Y. Li, H. W. Tseng, D. C. Ralph, and R. A. Buhrman, Spin-torque switching with the giant spin Hall effect of tantalum, Science **336**, 555 (2012).

[6] S. Fukami, T. Anekawa, C. Zhang, and H. Ohno, Collinear magnetic easy axis and current, Nat. Nanotechnol. **11**, 621 (2016).

[7] J. Kim, J. Sinha, M. Hayashi, M. Yamanouchi, S. Fukami, T. Suzuki, S. Mitani, and H. Ohno, Layer thickness dependence of the current-induced effective field vector in Ta|CoFeB|MgO, Nat. Mater. **12**, 240 (2013).

[8] C.-F. Pai, L. Liu, Y. Li, H. W. Tseng, D. C. Ralph, and R. A. Buhrman, Spin transfer torque devices utilizing the giant spin Hall effect of tungsten, Appl. Phys. Lett. **101**, 122404 (2012).

[9] S. Shi, Y. Ou, S. V. Aradhya, D. C. Ralph, and R. A. Buhrman, Fast Low-Current Spin-Orbit-Torque Switching of Magnetic Tunnel Junctions through Atomic Modifications of the Free-Layer Interfaces, Phys. Rev. Appl. **9**, 011002(R) (2018).

[10] E. Grimaldi, V. Krizakova, G. Sala, F. Yasin, S. Couet, G. Sankar Kar, K. Garello, and P. Gambardella, Single-shot dynamics of spin-orbit torque and spin transfer torque switching in three-terminal magnetic tunnel junctions, Nat. Nanotechnol. **15**, 111 (2020).

[11] T. Tanaka, H. Kontani, M. Naito, T. Naito, D. S. Hirashima, K. Yamada, and J. Inoue, Study of intrinsic spin Hall effect and orbital Hall effect in 4*d* and 5*d* transition metals, Phys. Rev. B **77**, 165117 (2008).

[12] K. Shahbazi, J.-V. Kim, H. T. Nembach, J. M. Shaw, A. Bischof, M. D. Rossell, V. Jeudy, T. A. Moore, and C. H. Marrows, Domain-wall motion and interfacial Dzyaloshinskii-Moriya interactions in Pt/Co/Ir(t_{Ir})/Ta multilayers, Phys. Rev. B **99**, 094409 (2019).

[13] K.-S. Ryu, S.-H. Yang, L. Thomas, and S. S. P. Parkin, Chiral spin torque arising from proximity-induced magnetization, Nat. Commun. **5**, 3910 (2014).

[14] Y. Ishikuro, M. Kawaguchi, N. Kato, Y.-C. Lau, and M. Hayashi, Dzyaloshinskii-Moriya interaction and spin-orbit torque at the Ir/Co interface, Phys. Rev. B **99**, 134421 (2019).

[15] H. Yang, S. Hu, M. Tang, S. Chen, H. Chen, D. Wu, and X. Qiu, Spin-orbit torque and Dzyaloshinskii-Moriya interaction in perpendicularly magnetized heterostructures with iridium, Appl. Phys. Lett. **118**, 062409 (2021).

[16] W. Zhang, M. B. Jungfleisch, W. Jiang, J. Sklenar, F. Y. Fradin, J. E. Pearson, J. B. Ketterson, and A. Hoffmann, Spin pumping and inverse spin Hall effects—insights for future spin-orbitronics (invited), J. Appl. Phys. **117**, 172610 (2015).

[17] T. Fache, J. C. Rojas-Sanchez, L. Badie, S. Mangin, and S. Petit-Watelot, Determination of spin Hall angle, spin mixing conductance, and spin diffusion length in CoFeB/Ir for spin-orbitronic devices, Phys. Rev. B **102**, 064425 (2020).

[18] Y. Liu, B. Zhou, and J.-G. Zhu, Field-free magnetization switching by utilizing the spin Hall effect and interlayer exchange coupling of iridium, Sci. Rep. **9**, 325 (2019).

[19] P. M. Haney, H.-W. Lee, K.-J. Lee, A. Manchon, and M. D. Stiles, Current induced torques and interfacial spin-orbit coupling: Semiclassical modeling, Phys. Rev. B **87**, 174411 (2013).

[20] Y.-T. Chen, S. Takahashi, H. Nakayama, M. Althammer, S. T. B. Goennenwein, E. Saitoh, and G. E. W. Bauer, Theory of spin Hall magnetoresistance, Phys. Rev. B **87**, 144411 (2013).

[21] G. Allen, S. Manipatruni, D. E. Nikonov, M. Doczy, and I. A. Young, Experimental demonstration of the coexistence of spin Hall and Rashba effects in β-tantalum/ferromagnet bilayers, Phys. Rev. B **91**, 144412 (2015).

[22] S. Emori, T. Nan, A. M. Belkessam, X. Wang, A. D. Matyushov, C. J. Babroski, Y. Gao, H. Lin, and N. X. Sun, Interfacial spin-orbit torque without bulk spin-orbit coupling, Phys. Rev. B **93**, 180402(R) (2016).

[23] L. Liu, T. Moriyama, D. C. Ralph, and R. A. Buhrman, Spin-Torque Ferromagnetic Resonance Induced by the Spin Hall Effect, Phys. Rev. Lett. **106**, 036601 (2011).

[24] M.-H. Nguyen, D. C. Ralph, and R. A. Buhrman, Spin Torque Study of the Spin Hall Conductivity and Spin Diffusion Length in Platinum Thin Films with Varying Resistivity, Phys. Rev. Lett. **116**, 126601 (2016).

[25] C.-F. Pai, Y. Ou, L. H. Vilela-Leão, D. C. Ralph, and R. A. Buhrman, Dependence of the efficiency of spin Hall torque on the transparency of Pt/ferromagnetic layer interfaces, Phys. Rev. B **92**, 064426 (2015).

[26] M. Hayashi, J. Kim, M. Yamanouchi, and H. Ohno, Quantitative characterization of the spin-orbit torque using harmonic Hall voltage measurements, Phys. Rev. B **89**, 144425 (2014).

[27] C. O. Avci, K. Garello, M. Gabureac, A. Ghosh, A. Fuhrer, S. F. Alvarado, and P. Gambardella, Interplay of spin-orbit torque and thermoelectric effects in ferromagnet/normal-metal bilayers, Phys. Rev. B **90**, 224427 (2014).

[28] N. Roschewsky, E. S. Walker, P. Gowtham, S. Muschinske, F. Hellman, S. R. Bank, and S. Salahuddin, Spin-orbit torque and Nernst effect in Bi-Sb/Co heterostructures, Phys. Rev. B **99**, 195103 (2019).

[29] See Supplemental Material at http://link.aps.org/supplemental/10.1103/PhysRevB.103.184416 for the details of fieldlike torque estimation.

[30] Y. Ou, C.-F. Pai, S. Shi, D. C. Ralph, and R. A. Buhrman, Origin of fieldlike spin-orbit torques in heavy metal/ferromagnet/oxide thin film heterostructures, Phys. Rev. B **94**, 140414(R) (2016).

[31] C.-F. Pai, M.-H. Nguyen, C. Belvin, L. H. Vilela-Leão, D. C. Ralph, and R. A. Buhrman, Enhancement of perpendicular magnetic anisotropy and transmission of spin-Hall-effect-induced spin currents by a Hf spacer layer in W/Hf/CoFeB/MgO layer structures, Appl. Phys. Lett. **104**, 082407 (2014).

[32] T. Nan, S. Emori, C. T. Boone, X. Wang, T. M. Oxholm, J. G. Jones, B. M. Howe, G. J. Brown, and N. X. Sun, Comparison of spin-orbit torques and spin pumping across NiFe/Pt and NiFe/Cu/Pt interfaces, Phys. Rev. B **91**, 214416 (2015).

[33] J. Kim, J. Sinha, S. Mitani, M. Hayashi, S. Takahashi, S. Maekawa, M. Yamanouchi, and H. Ohno, Anomalous temperature dependence of current-induced torques in CoFeB/MgO heterostructures with Ta-based underlayers, Phys. Rev. B **89**, 174424 (2014).

[34] K.-W. Kim, H.-W. Lee, K.-J. Lee, and M. D. Stiles, Chirality from Interfacial Spin-Orbit Coupling Effects in Magnetic Bilayers, Phys. Rev. Lett. **111**, 216601 (2013).

[35] L. Zhu and R. A. Buhrman, Absence of Significant Spin-Current Generation in Ti/Fe-Co-B Bilayers with Strong Interfacial Spin-Orbit Coupling, Phys. Rev. Appl. **15**, L031001 (2021).

[36] O. J. Lee, L. Q. Liu, C. F. Pai, Y. Li, H. W. Tseng, P. G. Gowtham, J. P. Park, D. C. Ralph, and R. A. Buhrman, Central role of domain wall depinning for perpendicular magnetization switching driven by spin torque from the spin Hall effect, Phys. Rev. B **89**, 024418 (2014).